

Ancient Alluvial Plains at Oxia Planum, Mars

Joel M. Davis¹, Matthew R Balme², Peter Fawdon², Peter Martin Grindrod³, Elena A Favaro², Steven G Banham⁴, and Nicolas Thomas⁵

¹Birkbeck, University of London

²Open University

³Natural History Museum

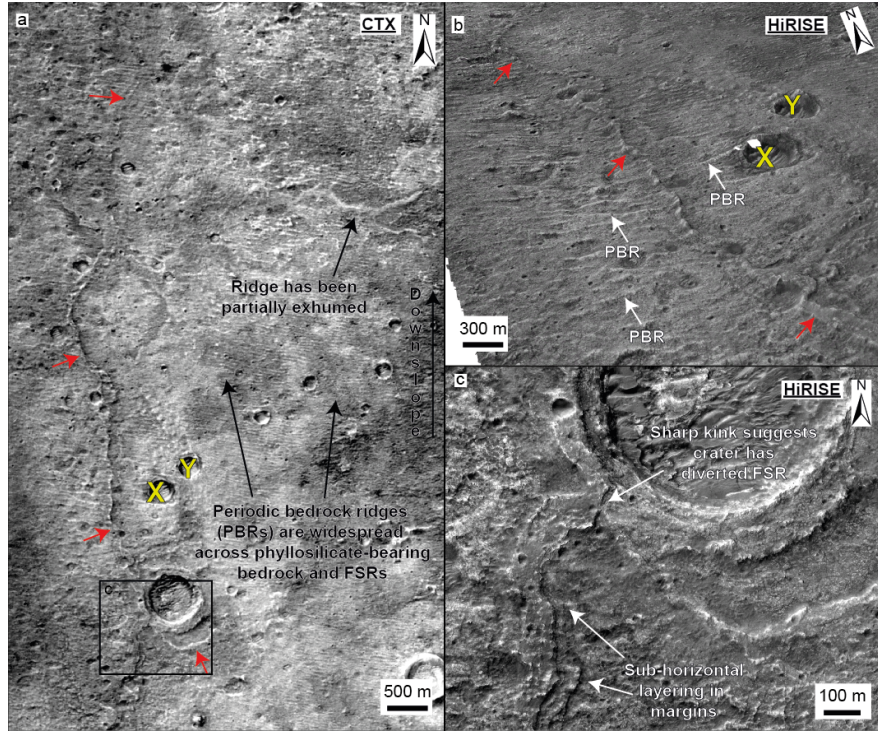
⁴Imperial College London

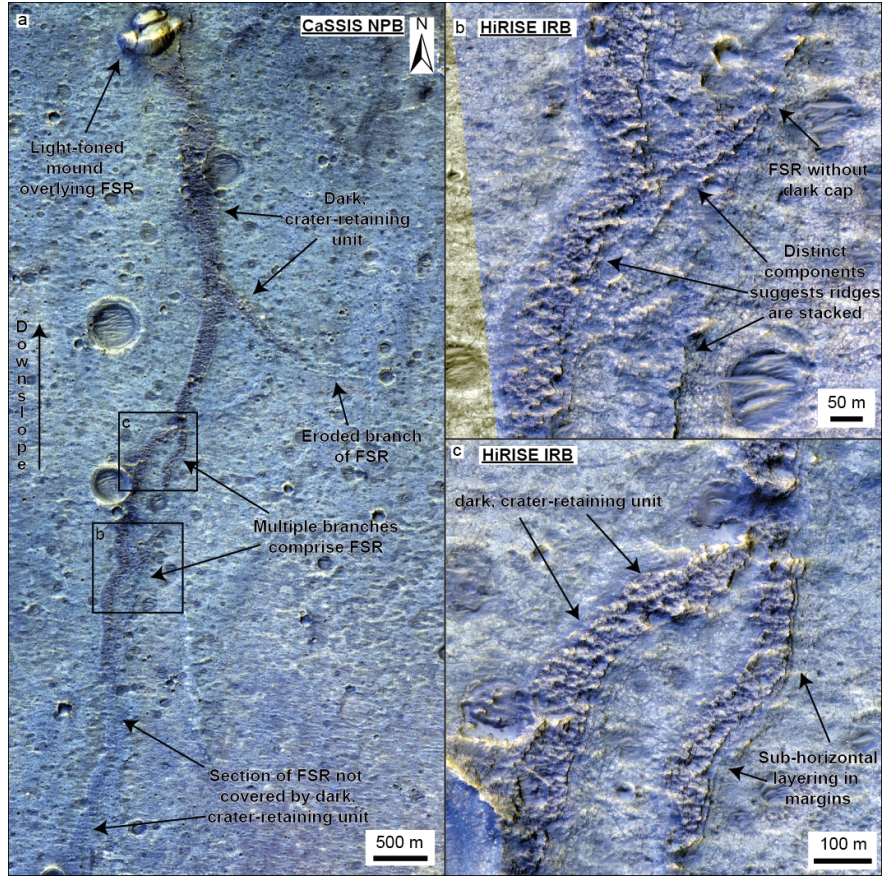
⁵University of Bern

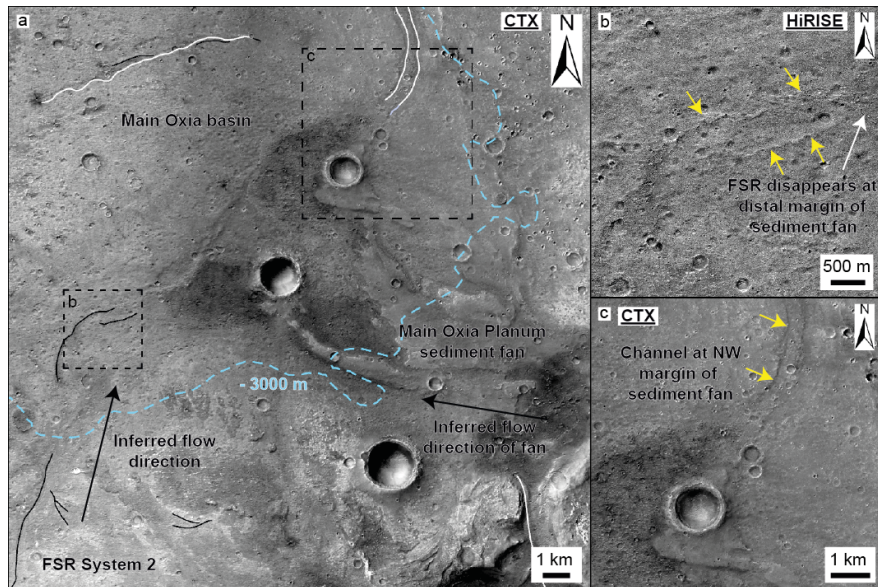
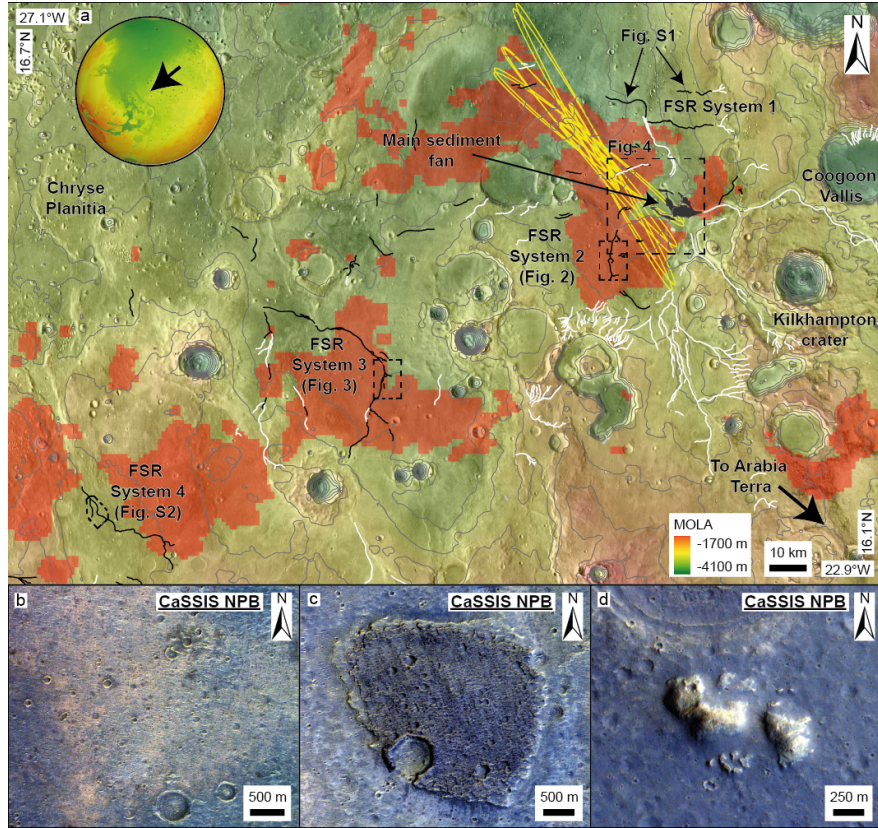
November 26, 2022

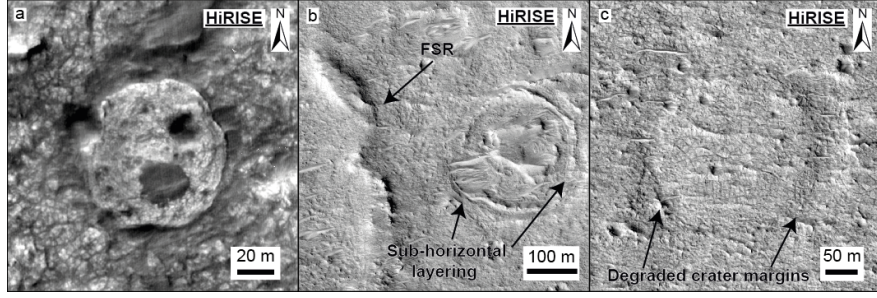
Abstract

The geologic origin of the ancient, phyllosilicate-bearing bedrock at Oxia Planum, Mars, the ExoMars rover landing site, is unknown. The phyllosilicates record ancient aqueous processes, but the processes that formed the host bedrock remain elusive. Here, we use high-resolution orbital and topographic datasets to investigate and characterize fluvial sinuous ridges (FSRs), found across the Oxia Planum region. The FSRs form segments up to 70 km long, with sub-horizontal layering common in ridge margins. Some FSRs comprise multi-story ridge systems; many are embedded within the phyllosilicate-bearing bedrock. We interpret the FSRs at Oxia Planum as deposits of ancient, episodically active, alluvial river systems (channel-belt and overbank deposits). Thus, the phyllosilicate-bearing bedrock was formed at least partly by ancient alluvial rivers, active across the wider region. Future exploration by the ExoMars rover can verify this interpretation and provides an opportunity to investigate some of the oldest river deposits in the Solar System.









Ancient Alluvial Plains at Oxia Planum, Mars

Joel M. Davis¹, Matthew R. Balme², Peter Fawdon², Peter M. Grindrod³, Elena A. Favaro²,
Steven G. Banham⁴, Nicolas Thomas⁵

¹Department of Earth and Planetary Sciences, Birkbeck, University of London, London, WC1E 7HX, UK

²School of Physical Sciences, The Open University, Milton Keynes, Buckinghamshire, MK7 7EA, UK

³Department of Earth Sciences, Natural History Museum, London, SW7 5BD, UK

⁴Department of Earth Sciences and Engineering, Imperial College London, London, SW7 2AZ, UK

⁵Physikalisches Institut, University of Bern, Sidlerstrasse 5, 3012 Bern, Switzerland

Key Points:

- Fluvial sinuous ridges (FSRs) are widespread across the Oxia Planum region, near the ExoMars rover landing site
- The FSRs suggest the phyllosilicate-bearing bedrock at the landing site comprises the deposits of ancient, alluvial river systems
- At Oxia Planum, the ExoMars rover could investigate some of the oldest preserved river deposits in the Solar System

21 **Abstract**

22 The geologic origin of the ancient, phyllosilicate-bearing bedrock at Oxia Planum, Mars,
23 the ExoMars rover landing site, is unknown. The phyllosilicates record ancient aqueous
24 processes, but the processes that formed the host bedrock remain elusive. Here, we use high-
25 resolution orbital and topographic datasets to investigate and characterize fluvial sinuous ridges
26 (FSRs), found across the Oxia Planum region. The FSRs form segments up to 70 km long, with
27 sub-horizontal layering common in ridge margins. Some FSRs comprise multi-story ridge
28 systems; many are embedded within the phyllosilicate-bearing bedrock. We interpret the FSRs at
29 Oxia Planum as deposits of ancient, episodically active, alluvial river systems (channel-belt and
30 overbank deposits). Thus, the phyllosilicate-bearing bedrock was formed at least partly by
31 ancient alluvial rivers, active across the wider region. Future exploration by the ExoMars rover
32 can verify this interpretation and provides an opportunity to investigate some of the oldest river
33 deposits in the Solar System.

34 **Plain Language Summary**

35 The ExoMars Rosalind Franklin rover will land at a region known as Oxia Planum on
36 Mars to look for signs of ancient life in the rock record. Phyllosilicate minerals are common at
37 Oxia Planum and are the main target of the mission because of their potential to preserve organic
38 molecules. However, how the host bedrock containing the phyllosilicate minerals formed is
39 unknown. Here, we use high-resolution image and topographic datasets from satellites to
40 investigate quasi-sinuuous ridges in the Oxia Planum region. The ridges form segments up to 70
41 km long and appear to be made of sedimentary rocks. The ridges are found on and are contained
42 within the phyllosilicate-bearing bedrock. We interpret the ridges as being formed by
43 depositional rivers at Oxia Planum, that were active billions of years ago. By extension, this
44 suggests that the formation of the phyllosilicate-bearing bedrock was associated with these
45 rivers, possibly representing ancient floodplains. Future exploration by the ExoMars rover can
46 verify this interpretation and provide an opportunity to investigate some of the oldest river
47 deposits in the Solar System.

48 **1 Introduction and the Geology of Oxia Planum**

49 The main objective of the European Space Agency (ESA) ExoMars “Rosalind Franklin”
50 rover mission is to search for evidence of past life on Mars (Vago et al., 2017). Noachian-aged,
51 phyllosilicate-bearing bedrock exposures at Oxia Planum, the landing site for the mission
52 (Quantin et al., 2021), forms the main sampling target as it provides strong evidence for ancient
53 aqueous processes and could potentially preserve organic material (Westall et al., 2015).
54 Although the phyllosilicates are widespread across the landing site, it is unclear whether they are
55 authigenic and/or detrital, or what processes formed the host bedrock (Quantin et al., 2021;
56 Mandon et al., 2021). Understanding the depositional process that formed these rocks and the
57 paleo-environmental conditions under which they were laid down, is critical for mission success.

58 Oxia Planum itself comprises a shallow topographic basin, situated on the margin of
59 hemispheric dichotomy of Mars, which divides the highlands of Arabia Terra to the southeast
60 from the Chryse Planitia lowlands to the northwest (Figure 1). The boundaries of the Oxia basin
61 may demarcate an ancient, highly degraded impact structure (Fawdon et al., 2021). The depth of
62 the phyllosilicate-bearing bedrock basin fill is unknown, but is at least 100 m in some areas
63 (Quantin et al., 2021). The Oxia Planum Fe/Mg phyllosilicates are part of the regionally

64 extensive circum-Chryse phyllosilicates, which are best exposed at Mawrth Vallis (e.g., Noe
65 Dobrea et al., 2010; Loizeau et al., 2007). Sub-horizontal, meter-scale layering, exposed in the
66 phyllosilicate-bearing bedrock at Oxia Planum generally points to a sedimentary origin, although
67 multiple formation hypotheses for the bedrock are also possible, including: large scale lava
68 flows, volcanoclastic deposits, impactogenic materials, aeolian deposits, or fluvio-lacustrine
69 deposits (Quantin et al., 2021; Mandon et al., 2021). Combined observations from the High
70 Resolution Imaging Science Experiment (HiRISE; McEwen et al., 2007), Colour and Stereo
71 Science Imaging System (CaSSIS; Thomas et al., 2017) and the Compact Reconnaissance
72 Imaging Spectrometer for Mars (CRISM; Murchie et al., 2007) divide the phyllosilicate-bearing
73 bedrock at Oxia Planum into at least two distinct sub-units, which may reflect compositional
74 variations: an underlying, orange-toned unit and an overlying, more olivine-rich, blue-toned unit
75 (Mandon et al., 2021; Parkes-Bowen et al., 2022).

76 At the eastern margins of the Oxia Planum landing ellipse is a 10 km long sediment fan
77 (Figure 1), previously interpreted as a delta, which likely formed in multiple stages (Quantin et
78 al., 2021; Molina et al., 2017). The fan is sourced from a regional highland catchment to the
79 southeast, including the extensive and long-lived Coogoon Vallis system (Fawdon et al., 2022;
80 Molina et al., 2017). The fan illustrates how fluvial processes might have transported detrital
81 phyllosilicates from the highland catchment into Oxia Planum, but is interpreted to postdate the
82 formation of the phyllosilicate-bearing bedrock (Quantin et al., 2021; Madon et al., 2021). Two
83 additional, geologically younger materials are found at Oxia: a dark-toned, crater-retaining unit
84 and a series of light-toned mounds. Both were probably once more extensive, suggesting that the
85 entire region has been subject to widespread and severe erosion (Quantin et al., 2021; McNeil et
86 al., 2021). The dark crater-retaining unit has previously been interpreted as an early Amazonian-
87 age volcanic unit (Quantin et al., 2021). The paleo-surface now represented by the mounds is
88 constrained by regional stratigraphic relationships to have formed in the early to middle
89 Noachian (McNeil et al., 2021).

90 Fawdon et al. (2022) identified several fluvial sinuous ridges (FSRs) in the Oxia basin,
91 providing further evidence for fluvial activity near the landing site. FSRs, or “inverted channels”,
92 are ridges of indurated, fluvially deposited sediment exhumed by differential erosion (e.g., Burr
93 et al., 2010; Williams et al., 2009; Davis et al., 2016). Examples on both Earth and Mars
94 demonstrate that FSRs may comprise either a single system channel-fill or deposits of migrating
95 and aggrading river channel-belts (e.g., Hayden et al., 2019; Davis et al., 2019; Balme et al.,
96 2020; Zaki et al., 2021). The latter are particularly relevant for understanding paleo-
97 environmental conditions as they may record multiphase depositional events over geologic
98 timescales. Having testable hypotheses ahead of the ExoMars rover landing is critical for any
99 time-limited investigations of the fluvial sinuous ridges performed on the surface. Here, we
100 explore the processes that the FSRs may record, their relationship to the phyllosilicate-bearing
101 bedrock, and the implications of their existence for its origin.

102 **2 Data and Methods**

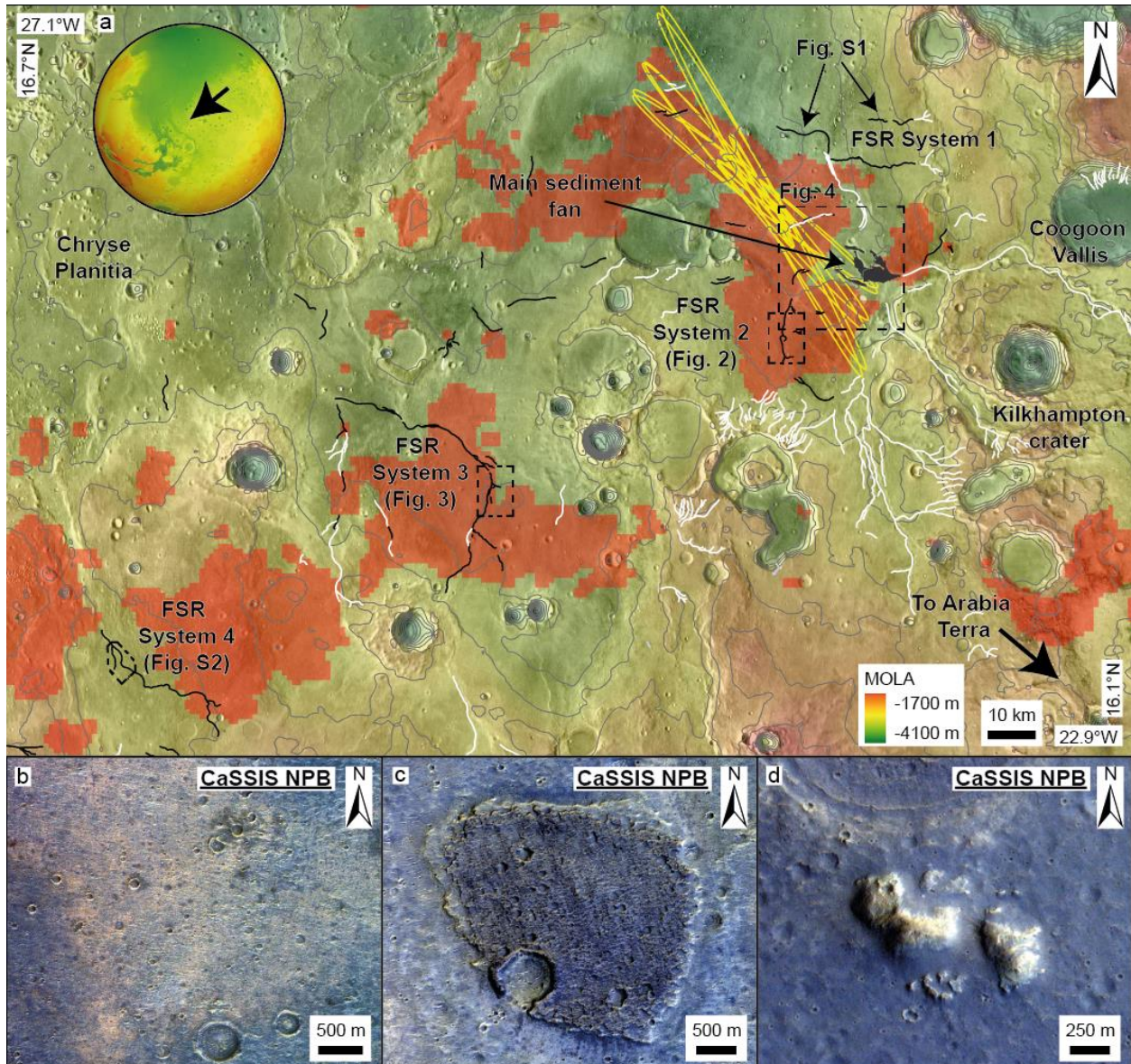
103 We investigated FSRs in Oxia Planum using orbital datasets including HiRISE (McEwen
104 et al., 2007), CaSSIS (Thomas et al., 2017), and Context Camera (CTX; Malin et al., 2007)
105 image and topographic datasets. We mapped the distribution of potential FSRs in the vicinity of
106 Oxia Planum onto a CTX mosaic basemap (6 m/pix) and accompanying digital elevation model
107 (DEM; 20 m/pix; Fawdon et al., 2021). Our mapping was supplemented by georeferenced

108 HiRISE and CaSSIS images where available and we built on the earlier map of Fawdon et al.
109 (2022). We investigated the morphology of the FSRs using a combination of panchromatic CTX
110 images, infrared-red-blue (IRB) and red only HiRISE images (0.25 m/pix), and near infrared-
111 panchromatic-blue (NPB) false color CaSSIS images (4.5 m/pix). Where possible, we generated
112 additional HiRISE and CTX DEMs using the USGS Integrated Software for Imagers and
113 Spectrometers (ISIS) software and the BAE photogrammetric package SOCET SET (Kirk et al.,
114 2008). In cases where SOCET SET failed to produce the DEM, we used the NASA Ames Stereo
115 Pipeline (Beyer et al., 2018). DEMs were tied to Mars Orbital Laser Altimeter (Zuber et al.,
116 1992) topography and exported with a post spacing of 20 m/pixel and 1 m/pixel for CTX and
117 HiRISE, respectively. These DEMs were supplemented with MOLA topography (463 m/pix).

118 **3 Observations**

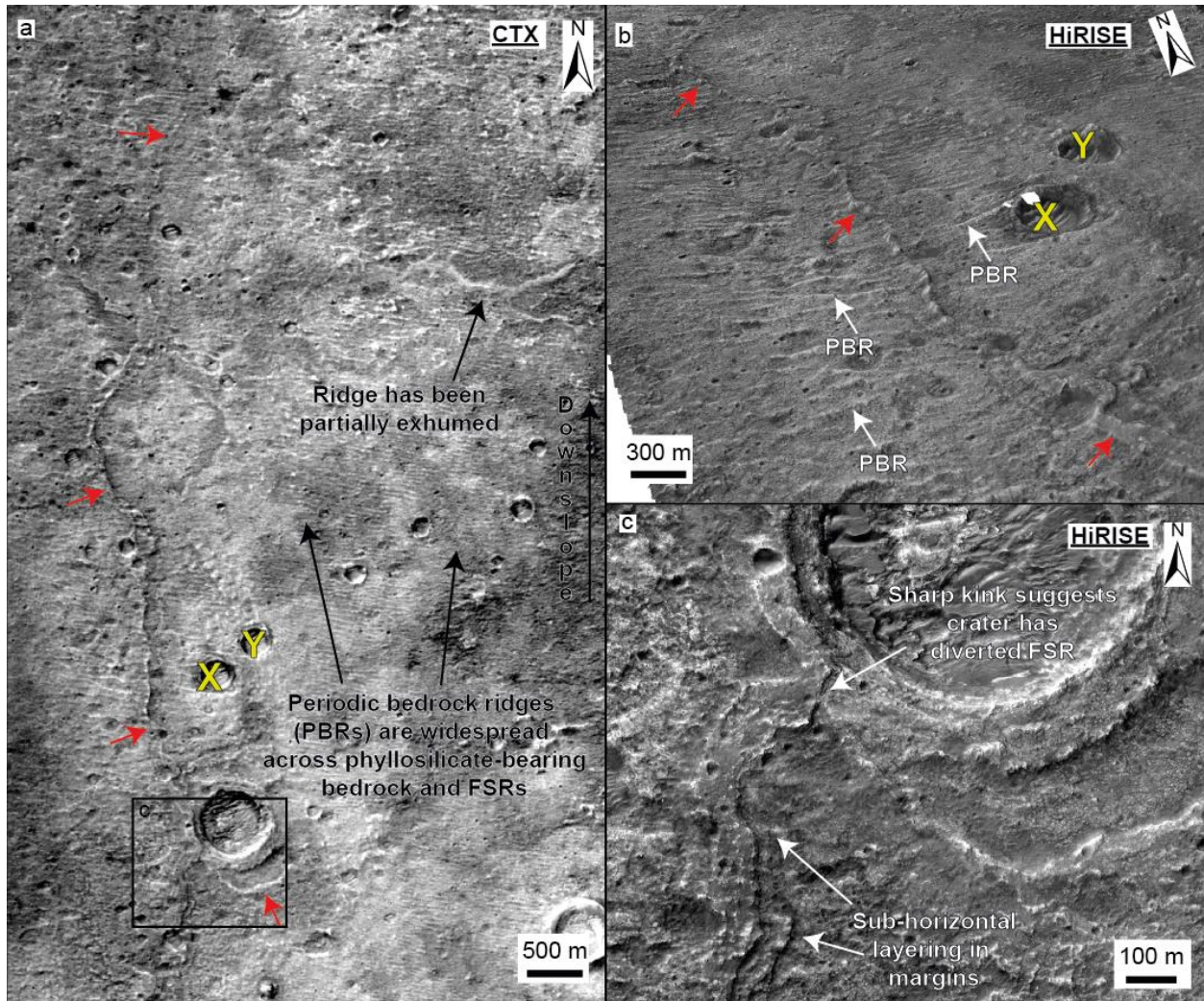
119 3.1 Catchment and Morphology of FSR systems

120 We define four FSR systems (from northeast to southwest, 1-4; Figure 1). They each
121 drain a region separate to the larger Coogoon Vallis catchment, which connects to the eastern
122 sediment fan (Fawdon et al., 2022). FSR system 1 is found within the eastern part of the landing
123 ellipse; all other systems occur south or southwest of the landing site, but in the same assemblage
124 of geologic materials. All four FSR systems also share the same morphologic characteristics:
125 they are straight to sinuous (sinuosity 1-1.4), tens to hundreds of meters wide (range is 20-600
126 m), and morphologically highly degraded (Figures 2, 3). Where suitable CTX or HiRISE
127 topography was available, the FSRs were measured to be 1-9 m above the adjacent bedrock. The
128 FSRs are mostly found in contiguous to semi-contiguous segments; the longest individual
129 segment is ~70 km. The FSRs are usually set within low relief plains or in subtle (meters deep),
130 approximately kilometer-wide valleys, and are often found downslope of more well-defined
131 erosional valleys (Figures 2, 3, S1, S2). The ridge trends are perpendicular to contour lines, with
132 their upslope ends being 100-200 m higher in elevation than the downslope ends (Figure 1). The
133 inferred paleoflow directions are broadly to the north or northwest, towards Chryse Planitia,
134 where the FSRs eventually become unrecognizable. Sub-horizontal, meter-scale layering is
135 clearly present in the margins of the FSRs, and grades into the adjacent and underlying terrain
136 (i.e., the phyllosilicate-bearing bedrock; Figures 2, 3). Beyond this, there is no discernable
137 sedimentary architecture recognizable in FSR margins at the scale of the available data.



138

139 Figure 1: (a) MOLA topographic map showing the distribution of fluvial sinuous ridges (FSRs;
 140 black solid lines) and fluvial valleys (white lines) in the Oxia Planum region. Detections of
 141 phyllosilicate minerals are shown in red (modified from Quantin et al., 2021). The ExoMars
 142 2022 landing ellipses are shown in yellow. Contours shown at 100 m intervals as fine grey lines.
 143 (b) CaSSIS image showing the phyllosilicate-bearing bedrock at Oxia Planum. (b) CaSSIS image of
 144 dark, crater-retaining unit. (c) CaSSIS image of light-toned mounds. Both the dark, crater-
 145 retaining unit and the light-toned mounds overlies the phyllosilicate-bearing bedrock. All image
 146 IDs for figures are provided in Table S2.



147

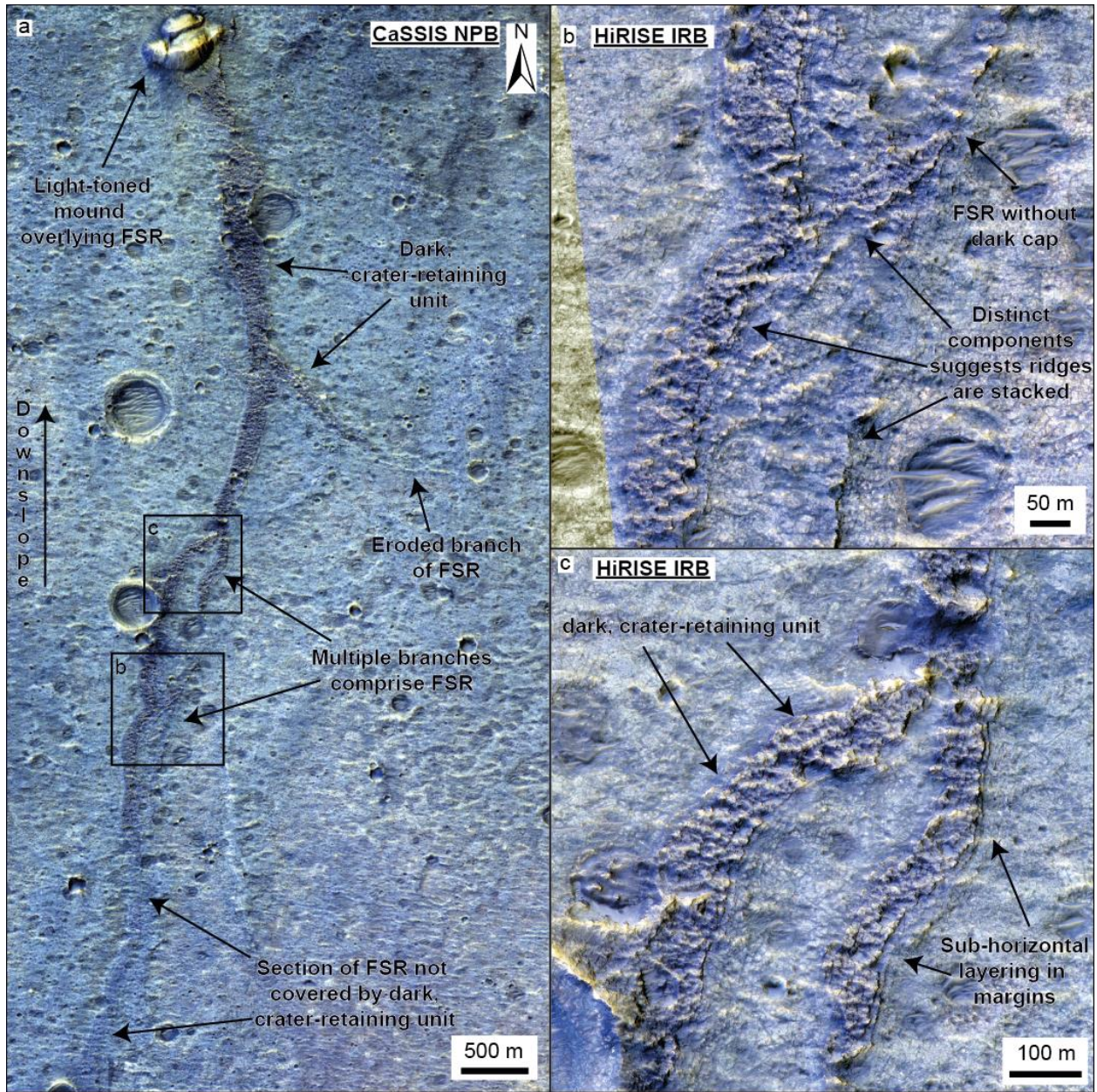
148 Figure 2. CTX and HiRISE images of FSR 2, south of the Oxia Planum landing ellipse. (a) CTX
 149 image showing ~10 km section of FSR (highlighted by red arrows). There are several examples
 150 of smaller ridges partially exhumed from the phyllosilicate-bearing bedrock. (b) Oblique HiRISE
 151 view of FSR (highlighted by red arrows) facing northeast (note X and Y are the same as in (a)).
 152 PBRs have eroded into both the phyllosilicate-bearing bedrock and the FSR. DEM constructed
 153 from ESP_069815_1975 and ESP_072017_1975. (c) HiRISE image showing section of FSR
 154 with a sharp kink around the impact crater, suggesting paleo-flow conformed to topography.

155 3.2 Relationship of FSRs to the Surrounding Terrain

156 A comparison of the FSR locations and previous detections of phyllosilicates in Oxia
 157 Planum (Carter et al., 2015; Quantin et al., 2021) demonstrates significant overlap (Figure 1).
 158 Most of the main and peripheral FSR systems are situated on or near detections of
 159 phyllosilicates. However, due to the limits of orbital detections, phyllosilicates are likely to be
 160 more abundant across the region than shown in Figure 1 (Murchie et al., 2007); certainly, the
 161 morphological characteristics of the phyllosilicate-bearing bedrock (e.g., light-toned, sub-
 162 horizontal layering, fractured) can be seen across areas that extend far beyond those with spectral
 163 phyllosilicate signatures (Quantin et al., 2021; Mandon et al., 2021). CaSSIS NPB and HiRISE

164 IRB images reveal that the FSRs are generally confined to the blue-toned (stratigraphically
165 higher) sub-unit of the phyllosilicate-bearing bedrock (Figure 3). Many FSR systems appear
166 partially exhumed from within the phyllosilicate-bearing bedrock (Figure 2, 3). Periodic bedrock
167 ridges (PBRs; Montgomery et al., 2012), parallel sets of aeolian-formed ridges eroded into
168 bedrock, previously identified across large parts of the phyllosilicate-bearing bedrock at Oxia
169 Planum (Silvestro et al., 2021; Favaro et al., 2021), are also superposed on several FSR systems
170 and the adjacent bedrock (Figure 2). FSR system 2, south of the landing site is overlain by the
171 eastern sediment fan (Figure 4).

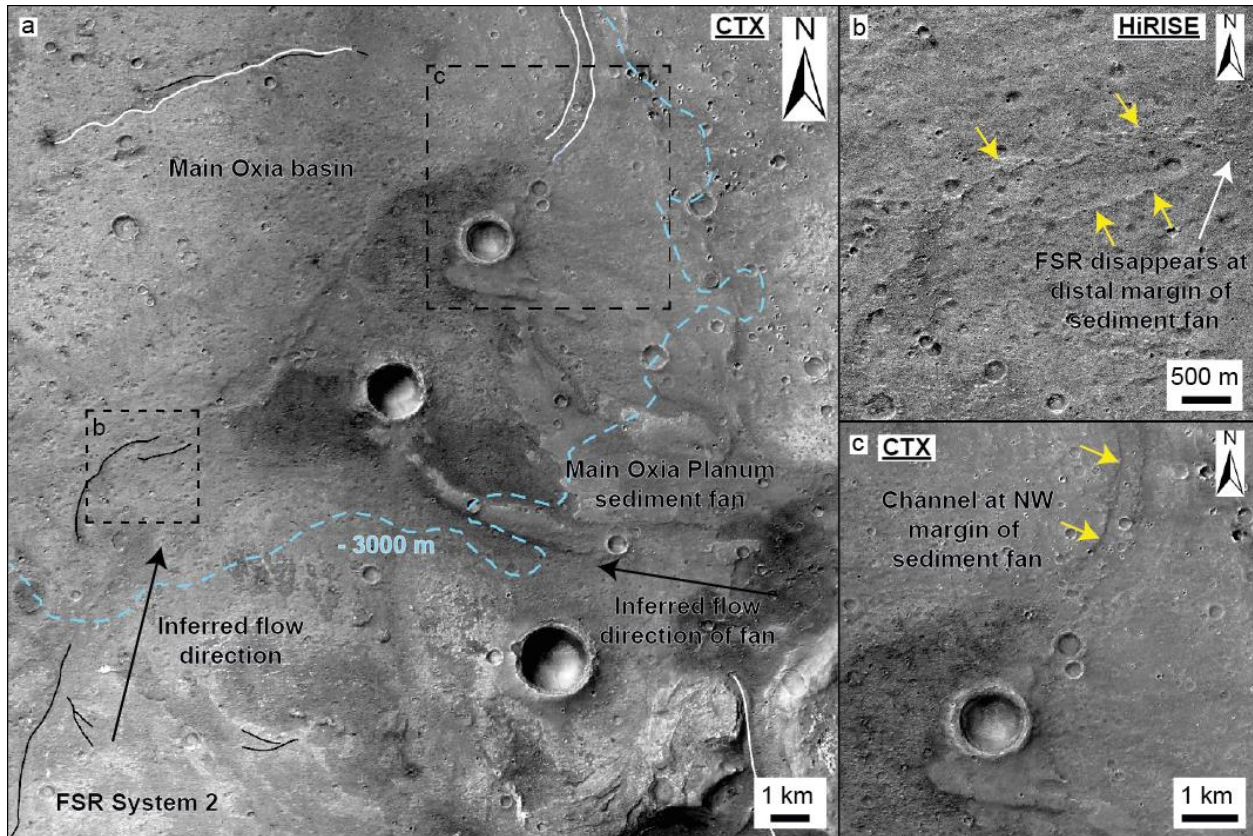
172 Generally, FSR pathways conform to the local topography, except where they are
173 deformed by tectonic wrinkle ridges; there are examples of FSRs converging on degraded impact
174 craters, only to be sharply diverted around them on approach (Figure 2c). Additionally, shallow,
175 degraded, impact craters (typically < 500 m diameter), which have formed into the
176 phyllosilicate-bearing bedrock adjacent to the FSRs, are commonly infilled (Figures 5, S3). In
177 some cases, the infill comprises light-toned, concentric layered deposits (Figures 5a, b); in
178 others, craters have been filled and/or buried almost entirely (Figure 5c). Similar infill is not
179 present in less degraded, fresher impact craters (i.e., those with preserved ejecta and well-defined
180 rims). Some of the FSR systems appear covered by the regionally recurrent, dark crater-retaining
181 unit (Quantin et al., 2021). However, we note that (1) this coverage is not continuous along the
182 entire length of FSRs and (2) in places, the dark crater-retaining unit has been eroded back,
183 revealing a distinct, underlying ridge structure (Figure 3). This is particularly apparent in CaSSIS
184 and HiRISE images (Figure 3). Like other examples, these FSRs also bear similarities in tone,
185 color, and texture, to the phyllosilicate-bearing bedrock, while the dark crater-retaining unit
186 generally appears to be of limited vertical thickness (~1 m). We note that this is also the case for
187 other regional examples of FSRs, outside of Oxia Planum. One example, FSR system 3, is
188 superposed by light-toned mounds (McNeil et al., 2021), potentially putting a lower age limit on
189 FSR formation (Figure 3).



190

191 Figure 3. CaSSIS and HiRISE images of FSR System 3 southwest of Oxia Planum landing
 192 ellipse. (a) CaSSIS NPB image showing FSR with multiple branches set within the
 193 phyllosilicate-bearing bedrock. (b) HiRISE IRB image showing section of FSR. Here, multiple
 194 vertically stacked ridges are present and in places, the FSR is not covered by the dark crater-

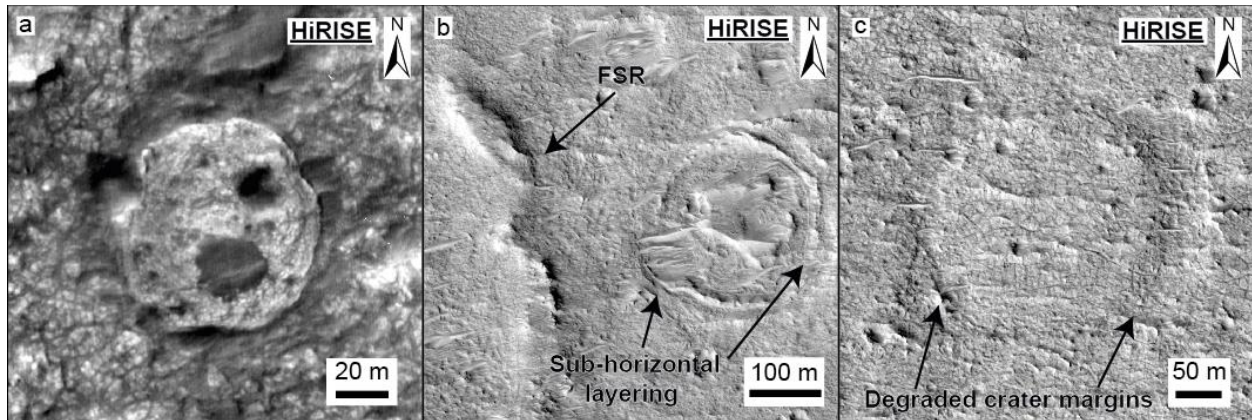
195 retaining unit. (c) HiRISE IRB showing section of FSR covered by dark, crater-retaining unit.
 196 However, sub-horizontal layering is still visible in the FSR margins.



197

198 Figure 4. (a) CTX mosaic showing the delta-like sediment fan at the eastern margin of Oxia
 199 Planum. The inferred paleo-flow direction of FSR system 2 contrasts with that of the delta-like
 200 sediment fan (b) HiRISE image showing that FSR system 2 (yellow arrows) disappears as it
 201 approaches the distal margin of the sediment fan, suggesting it is buried by the fan. (c) CTX

202 image showing a channel (yellow arrows) emerging at the NW margin of the sediment fan,
 203 possible a continuation of FSR system 2.



204

205 Figure 5. HiRISE images showing craters within the phyllosilicate-bearing bedrock that have
 206 been infilled with light-toned layered deposits, and in some cases buried entirely, adjacent to and
 207 associated with the FSRs.

208

209 4 Discussion

210 4.1 Interpretation of the Fluvial Sinuous Ridges

211 We interpret the FSRs as exhumed fluvial deposits. The FSRs are morphologically
 212 distinct from large-scale tectonic wrinkle ridges, which have deformed the region. Also, there are
 213 no recognizable glacial landforms associated with the FSRs, making an esker interpretation
 214 unlikely (Butcher et al., 2021). We note that no FSRs are set within deep bedrock valleys;
 215 instead, they are found on low-relief plains (the phyllosilicate-bearing bedrock; Figures 2, 3, S1a,
 216 S2) or set within or downslope of shallow valleys (Figure S1b). The FSRs therefore likely
 217 represent the deposits of ancient, alluvial river systems that traversed the plains at and around
 218 Oxia Planum (e.g., Hayden et al., 2019; Davis et al., 2019; Balme et al., 2020; Zaki et al., 2021),
 219 rather than erosive rivers incised into bedrock. Secondary ridges associated with and converging
 220 on the main systems could be either tributaries or earlier generations of rivers which are in
 221 different states of exhumation, or both.

222 The sub-horizontal layering in the FSRs (Figures 2, 3) and examples of both partially
 223 exhumed and superposing ridge systems (i.e., ridge stacking; Figure 3b) argues against simple
 224 channel-fill, deposited in a single event, composing the ridges. These characteristics instead
 225 support an interpretation of the FSRs as the remains of channel-belt and floodplain deposits. The
 226 concentric layered deposits in impact craters adjacent to the FSRs may record overbank
 227 deposition and/or ponding in local accommodation (Figures 5, S3). Some of the FSRs have
 228 previously been interpreted as erosional channels that were later and exclusively filled by the
 229 dark crater-retaining unit (i.e., non-fluvially deposited material; Quantin et al., 2021). However,
 230 the observations that this material is generally thin and, in places, has been eroded back to reveal
 231 a distinct, underlying, layered ridge structure, invalidates this interpretation in at least these

232 examples (Figure 3). Instead, most of the ridge structure of the FSRs appears to be embedded
233 within and exhumed from the phyllosilicate-bearing bedrock itself (Figures 2, 3).

234 4.2 Constraints on Phyllosilicate-Bearing Bedrock Formation

235 We note that most of the FSRs are found outside the landing ellipse (Figure 1). However,
236 due to the inherent nature of migratory river systems and the erosional processes that expose
237 them in the rock record, it is unlikely that the FSRs as they are currently exposed represent the
238 full extent of alluvial river systems at Oxia Planum, both spatially and vertically within the
239 stratigraphy. Furthermore, the similar morphological characteristics on the phyllosilicate-bearing
240 bedrock throughout the region points to common formational processes. Thus, we suggest that at
241 least some of the phyllosilicate-bearing bedrock comprises alluvial (both channel-belt and
242 floodplain) deposits; this may be the case throughout the landing ellipse and the wider region.
243 The low relief (< 10 m) and poor exposure of the FSRs across the Oxia Planum landscape may
244 be due to a high mudstone fraction in the bedrock, which led to moderate differential erosion
245 producing more subdued topography than is typical of other landscapes containing FSRs (e.g.,
246 Davis et al., 2019; Zaki et al., 2021). The FSR height (1-9 m) reveals the minimum vertical
247 thickness of alluvial deposits at Oxia Planum; the true thickness of alluvial deposits is likely be
248 greater. These ancient rivers provide one mechanism for the erosion, transport, and deposition of
249 sediment in Oxia Planum. The upland catchment from which these rivers seem to originate
250 (Fawdon et al., 2022), and the presence of impact craters which have altered their pathways
251 within Oxia Planum, suggest that sediment was sourced both regionally in the highlands and
252 locally from the phyllosilicate-bearing bedrock itself, before being deposited elsewhere.

253 The presence of embedded and partially filled impact craters in the phyllosilicate-bearing
254 bedrock (Figure 5, S3) points to substantive hiatuses in bedrock deposition and the formation of
255 paleo-surfaces (e.g., Kite et al., 2017), followed by a later resumption in depositional processes.
256 Thus, if alluvial river systems were responsible for the deposition of sedimentary bedrock here,
257 they were probably episodically active, although the presence of stacked channel deposits (e.g.,
258 Figure 3) suggests these episodes consisted of sustained aggradation (Colombera et al., 2015).
259 The association of the FSRs with the blue-toned sub-unit of the phyllosilicate-bearing bedrock, is
260 consistent with episodic activity, where the presence of olivine points to limited aqueous
261 alteration (Mandon et al., 2021). Furthermore, Fawdon et al. (2022) identified two major phases
262 of fluvial activity separated by a substantial hiatus in the regional Coogoon Vallis system. Our
263 interpretation does not constrain the origin of the phyllosilicates themselves as detrital or
264 authigenic. If phyllosilicate-bearing sediments were present when these ancient river systems
265 were active, the phyllosilicate minerals might have contributed to the stability of their banks
266 (e.g., Lapôtre et al., 2019). Our alluvial hypothesis does not exclude other sources of sediment
267 playing a role in building the terrain as well (e.g., volcaniclastic, aeolian, impactogenic; Quantin
268 et al., 2021; Mandon et al., 2021).

269 4.3 Testing the Alluvial Hypothesis with the ExoMars rover

270 Our interpretation of an ancient alluvial environment can be reconciled with the former
271 presence of a standing body of water at Oxia Planum, previously interpreted from the presence of
272 a delta-like sediment fan at the end of Coogoon Vallis (Quantin et al., 2021; Molina et al., 2017).
273 It is likely that these different paleo-environments existed at separate times; indeed, Quantin et
274 al. (2021) suggest the delta-like sediment fan formed after the phyllosilicate-bearing bedrock

275 (which contains the FSRs). Furthermore, investigations of terrestrial FSRs have shown that they
276 can record multiple paleo-environments not apparent in planimetric pattern. For example, in the
277 Californian Mojave Desert, Miller et al. (2018) document multiple examples of lake-rise pulses
278 contained within inverted paleochannels (i.e., FSRs) associated with the southern Lake Coyote in
279 the late Quaternary. The lake-rise pulses cover a period of ~10 ka and were identified from
280 radiocarbon dating of lacustrine fossils, but importantly were not recognizable in the ridge
281 structure from orbital data (Miller et al., 2018). A similar scenario at Oxia Planum is possible
282 and evidence for lacustrine episodes recorded within the FSRs might only be revealed by in situ
283 investigations.

284 Our predictions of an ancient alluvial landscape in Oxia Planum can be readily tested by
285 the ExoMars rover. If widespread alluvial plains are present at Oxia Planum, diagnostic outcrops
286 and lithologies such as conglomerates may be present. This is the case in the plains surrounding
287 Mount Sharp in Gale crater, as imaged by the Curiosity rover (William et al., 2013; Grotzinger et
288 al., 2014), despite there being little evidence of an ancient alluvial environment from orbital data.
289 If, for example, similar fine-pebble conglomerates (2-40 mm coarse grain size range) occur at the
290 Oxia Planum landing site, they would be identifiable at working distances of up to 50 m by
291 ExoMars' Panoramic Camera instrument, using its High Resolution Camera (Coates et al.,
292 2017). Grain sizes measured from such outcrops could be used for paleo-hydrologic
293 reconstructions (William et al., 2013), potentially revealing Noachian flow conditions.

294 Due to the rapid burial of sediment, alluvial floodplains and lacustrine environments are
295 considered to have moderate to high preservation potential for organic matter (Summons et al.,
296 2011). Thus, as phyllosilicate-bearing bedrock with morphology identical to the FSR-bearing
297 surface shown here is widespread in the landing ellipse, our interpretation increases the
298 likelihood that the ExoMars rover will encounter habitable paleoenvironments and meet its main
299 mission objective of detecting ancient life. Finally, given the ancient age of the phyllosilicate-
300 bearing bedrock (~ 4 Ga; Quantin et al., 2021), if the alluvial hypothesis is correct, the ExoMars
301 rover may provide the opportunity to investigate in situ some of the oldest preserved river
302 deposits in the Solar System.

303 **Acknowledgments**

304 Support from the UK Space Agency is gratefully acknowledged (JMD: ST/R002355/1;
305 ST/V002678/1; ST/W002566/1, MRB: ST/T002913/1, ST/V001965/1; ST/R001413/1, PF;
306 ST/W002736/1). We thank the various Mars instrument science and engineering teams for their
307 consistently excellent and dedicated work. We thanks Susan Conway and Axel Noblet for
308 assistance with DEM production. CaSSIS is a project of the University of Bern and funded
309 through the Swiss Space Office via ESA's PRODEX programme. The instrument hardware
310 development was also supported by the Italian Space Agency (ASI) (ASI-INAF agreement
311 no.I/018/12/0), INAF/Astronomical Observatory of Padova, and the Space Research Center
312 (CBK) in Warsaw. Support from SGF (Budapest), the University of Arizona (Lunar and
313 Planetary Lab.) and NASA are also gratefully acknowledged. Operations support from the UK
314 Space Agency under grant ST/R003025/1 is also acknowledged.

315

316 **Open Research**

317 The standard data products used here are available from the NASA Planetary Data
 318 System as follows. (1) HiRISE: <https://hirise-pds.lpl.arizona.edu/PDS/>; (McEwen, 2006). (2)
 319 CTX: <https://pds-imaging.jpl.nasa.gov/volumes/mro.html>; (Malin, 2007). (3) MOLA: <https://pds-geosciences.wustl.edu/missions/mgs/megdr.html>; (Neumann et al., 2003). CaSSIS data are
 320 available through the ESA Planetary Science Archive
 321 (<http://archives.esac.esa.int/psa/#!Table%20View/CaSSIS=instrument>). The CTX DEM mosaic
 322 of Oxia Planum is available at <https://doi.org/10.21954/ou.rd.16451220.v1>. One HiRISE DEM
 323 used is available on the HiRISE PDS. All other CTX and HiRISE Digital Elevation Models and
 324 shapefiles created for this project are available at
 325 <https://doi.org/10.6084/m9.figshare.c.6011638.v1>.

327 References

- 328 Balme, M. R., Gupta, S., Davis, J. M., Fawdon, P., Grindrod, P. M., Bridges, J. C., et al. (2020).
 329 Aram Dorsum: An extensive mid-Noachian age fluvial depositional system in Arabia
 330 Terra, Mars. *Journal of Geophysical Research: Planets*, 125, e2019JE006244.
 331 <https://doi.org/10.1029/2019JE006244>
- 332 Beyer, R. A., Alexandrov, O., & McMichael, S. (2018). The Ames Stereo Pipeline: NASA's
 333 Open Source Software for Deriving and Processing Terrain Data. *Earth and Space
 334 Science*, 5(9), 537–548. <https://doi.org/10.1029/2018EA000409>
- 335 Burr, D. M., Williams, R. M. E., Wendell, K. D., Chojnacki, M., & Emery, J. P. (2010). Inverted
 336 fluvial features in the Aeolis/Zephyria Plana region, Mars: Formation mechanisms and
 337 initial paleodischarge estimates. *Journal of Geophysical Research*, 115(E7), E07011.
 338 <https://doi.org/10.1029/2009JE003496>
- 339 Carter, J., Loizeau, D., Mangold, N., Poulet, F., & Bibring, J.-P. (2015). Widespread surface
 340 weathering on early Mars: A case for a warmer and wetter climate. *Icarus*, 248, 373– 382.
 341 <https://doi.org/10.1016/j.icarus.2014.11.011>
- 342 Butcher, F. E. G., Balme, M. R., Conway, S. J., Gallagher, C., Arnold, N. S., Storrar, R. D., et al.
 343 (2021). Sinuous ridges in Chukhung crater, Tempe Terra, Mars: Implications for fluvial,
 344 glacial, and glaciofluvial activity. *Icarus*, 357(September 2020), 114131.
 345 <https://doi.org/10.1016/j.icarus.2020.114131>
- 346 Coates A.J., Jaumann R., Griffiths A.D., Leff C.E., Schmitz N., Josset J.-L., et al., (2017) The
 347 PanCam Instrument for the ExoMars Rover. *Astrobiology* 17:511–541,
 348 <https://doi.org/10.1089/ast.2016.1548>
- 349 Colombera, L., Moutney, N. P., & McCaffrey, W. D. (2015). A meta-study of relationships
 350 between fluvial channel-body stacking pattern and aggradation rate: Implications for
 351 sequence stratigraphy. *Geology*, 43, 283–286. <https://doi.org/10.1130/G36385>.
- 352 Davis, J. (2022): Digital Elevation Models and Shapefiles - Oxia Planum Region, Mars. figshare.
 353 Collection. <https://doi.org/10.6084/m9.figshare.c.6011638.v1>
- 354 Davis, J.M., Balme, M., Grindrod, P.M., Williams, R.M.E., Gupta, S., 2016. Extensive Noachian
 355 fluvial systems in Arabia Terra: Implications for early Martian climate. *Geology* 44, 847–
 356 850. <https://doi.org/10.1130/G38247.1>

- 357 Davis, J.M., Gupta, S., Balme, M.R., Grindrod, P.M., Fawdon, P., Dickeson, Z.I., Williams,
358 R.M.E., 2019. A Diverse Array of Fluvial Depositional Systems in Arabia Terra:
359 Evidence for mid-Noachian to Early Hesperian Rivers on Mars. *J. Geophys. Res. Planets*
360 124, 1913–1934. <https://doi.org/10.1029/2019JE005976>
- 361 Favaro, E.A., M.R. Balme, J.M. Davis, P.M. Grindrod, P. Fawdon, A.M. Barrett, and S.R. Lewis
362 (2021), The Aeolian Environment of the Landing Site for the ExoMars Rosalind Franklin
363 Rover in Oxia Planum, Mars, *Journal of Geophysical Research Planets*, 126,
364 e2020JE006723, <https://doi.org/10.1029/2020JE006723>.
- 365 Fawdon, P., Grindrod, P., Orgel, C., Sefton-Nash, E., Adeli, S., Balme, M., et al., 2021. The
366 geography of Oxia Planum. *J. Maps* 17, 762–778.
367 <https://doi.org/10.1080/17445647.2021.1982035>
- 368 Fawdon, P., M.R. Balme, J.M. Davis, J.C. Bridges, S. Gupta, C. Quantin-Nataf (2022), Rivers
369 and lakes in Western Arabia Terra: The fluvial catchment of ExoMars rover landing site,
370 *J. Geophys. Res. Planets*, 27, e2021JE007045, <https://doi.org/10.1029/2021JE007045>.
- 371 Grotzinger, J. P., Sumner, D., Kah, L., Stack, K., Gupta, S., Edgar, L., et al. 2014, A habitable
372 fluvio-lacustrine environment at Yellowknife Bay, Gale Crater, Mars: *Science*, 343,
373 1242777, <https://doi.org/10.1126/science.1242777>
- 374 Hayden, A.T., Lamb, M.P., Fischer, W.W., Ewing, R.C., McElory, B.J., & Williams, R.M.E.
375 (2019). Formation of sinuous ridges by inversion of river-channel belts in Utah, USA,
376 with implications for Mars. *Icarus*. <https://doi.org/10.1016/j.icarus.2019.04.019>.
- 377 Kirk, R. L., Howington-Kraus, E., Rosiek, M. R., Anderson, J. A., Archinal, B. A., Becker, K. J.,
378 et al. (2008). Ultrahigh resolution topographic mapping of Mars with MRO HiRISE
379 stereo images: Meter-scale slopes of candidate Phoenix landing sites. *Journal of*
380 *Geophysical Research*, 113, E00A24. <https://doi.org/10.1029/2007JE003000>
- 381 Kite, E.S., Sneed, J., Mayer, D.P., and Wilson, S.A., 2017, Persistent or repeated surface
382 habitability on Mars during the late Hesperian–Amazonian: *Geophysical Research*
383 *Letters*, 44, 3991–3999, <https://doi.org/10.1002/2017GL072660>
- 384 Lapôtre, M. G. A., Ielpi, A., Lamb, M. P., Williams, R. M. E., & Knoll, A. H. (2019). Model for
385 the Formation of Single-Thread Rivers in Barren Landscapes and Implications for Pre-
386 Silurian and Martian Fluvial Deposits. *Journal of Geophysical Research: Earth Surface*,
387 124(12), 2757–2777. <https://doi.org/10.1029/2019JF005156>
- 388 Loizeau, D., Mangold, N., Poulet, F., Bibring, J. P., Gendrin, A., Ansan, V., et al. (2007).
389 Phyllosilicates in the Mawrth Vallis region of Mars. *Journal of Geophysical Research*,
390 112(8), 1–20. <https://doi.org/10.1029/2006je002877>
- 391 Malin, M. C. (2007). MRO Context Camera experiment data record level 0 v1.0. [Data set].
392 NASA Planetary Data System. <https://doi.org/10.17189/1520266>
- 393 Malin, M. C., Bell, J. F., Cantor, B. A., Caplinger, M. A., Calvin, W. M., Clancy, R. T., et al.
394 (2007). Context camera investigation on board the Mars reconnaissance orbiter. *Journal*
395 *of Geophysical Research*, 112, 1–25. <https://doi.org/10.1029/2006je002808>

- 396 Mandon, L., Parkes Bowen, A., Quantin-Nataf, C., Bridges, J.C., Carter, J., Pan, L., et al. 2021.
397 Morphological and Spectral Diversity of the Clay-Bearing Unit at the ExoMars Landing
398 Site Oxia Planum. *Astrobiology* 21, 464–480. <https://doi.org/10.1089/ast.2020.2292>
- 399 McEwen, A. S. (2006). MRO Mars High Resolution Image Science Experiment RDR V1.0.
400 [Data set]. NASA Planetary Data System. <https://doi.org/10.17189/1520303>
- 401 McEwen, A. S., Eliason, E. M., Bergstrom, J. W., Bridges, N. T., Hansen, C. J., Delamere, W.
402 A., et al. (2007). Mars reconnaissance orbiter's high resolution imaging science
403 experiment (HiRISE). *Journal of Geophysical Research*, 112(5), 1–40.
404 <https://doi.org/10.1029/2005je002605>. <https://doi.org/10.1029/2005JE002605>
- 405 McNeil, J.D., Fawdon, P., Balme, M.R., Coe, A.L., 2021. Morphology, Morphometry and
406 Distribution of Isolated Landforms in Southern Chryse Planitia, Mars. *J. Geophys. Res.*
407 *Planets* n/a, e2020JE006775. <https://doi.org/10.1029/2020JE006775>
- 408 Miller, D. M., Dudash, S. L., & McGeehin, J. P. (2018). Paleoclimate record for Lake Coyote,
409 California, and the Last Glacial Maximum and deglacial paleohydrology (25 to 14 cal ka)
410 of the Mojave River. In S. W. Starratt, & M. R. Rosen (Eds.), *From saline to freshwater:*
411 *The diversity of western lakes in space and time*, Special Paper, (Vol. 536, pp. 1–20).
412 Boulder, CO: Geological Society of America. [https://doi.org/10.1130/2018.2536\(12\)](https://doi.org/10.1130/2018.2536(12))
- 413 Molina, A., López, I., Prieto-Ballesteros, O., Fernández-Remolar, D., de Pablo, M.Á., Gómez,
414 F., 2017. Coogoon Valles, western Arabia Terra: Hydrological evolution of a complex
415 Martian channel system. *Icarus* 293, 27–44. <https://doi.org/10.1016/j.icarus.2017.04.002>
- 416 Montgomery, D. R., Bandfield, J. L., & Becker, S. K. (2012). Periodic bedrock ridges on Mars.
417 *Journal of Geophysical Research: Planets*, 117(E3), E03005.
418 <https://doi.org/10.1029/2011JE003970>
- 419 Murchie, S., Arvidson, R., Bedini, P., Beisser, K., Bibring, J.-P., Bishop, et al., 2007, Compact
420 Reconnaissance Imaging Spectrometer for Mars (CRISM) on Mars Reconnaissance
421 Orbiter (MRO): *Journal of Geophysical Research*, v. 112, E05S03, doi:
422 10.1029/2006JE002682.
- 423 Neumann, G., Zuber, M., & Smith, D. E. (2003). MOLA mission experiment gridded data
424 record. [Data set]. NASA Planetary Data System. <https://doi.org/10.17189/1519460>
- 425 Noe Dobra, E. Z., Bishop, J. L., McKeown, N. K., Fu, R., Rossi, C. M., Michalski, J. R., et al.
426 (2010). Mineralogy and stratigraphy of phyllosilicate-bearing and dark mantling units in
427 the greater Mawrth Vallis/west Arabia Terra area: Constraints on geological origin.
428 *Journal of Geophysical Research*, 115. <https://doi.org/10.1029/2009je003351>
- 429 Parkes Bowen, A., Bridges, J. C., Tornebene, L., Mandon, L., Quantin-Nataf, C., Patel, M. R., et
430 al. (2022). A CaSSIS and HiRISE map of the Clay-bearing Unit at the ExoMars 2022
431 landing site in Oxia Planum. *Planetary and Space Science*, 214, 105429,
432 <https://doi.org/10.1016/j.pss.2022.105429>
- 433 Quantin-Nataf, C., Carter, J., Mandon, L., Thollot, P., Balme, M., Volat, M., et al. (2021). Oxia
434 Planum: The landing site for the ExoMars “Rosalind Franklin” Rover Mission:
435 Geological context and prelanding interpretation. *Astrobiology*, 21.
436 <https://doi.org/10.1089/ast.2019.2191>

- 437 Silvestro, S., Pacifici, A., Salese, F., Vaz, D. A., Neesemann, A., Tirsch, D., et al. (2021).
438 Periodic Bedrock Ridges at the ExoMars 2022 Landing Site: Evidence for a Changing
439 Wind Regime. *Geophysical Research Letters*, 48(4), 1–10.
440 <https://doi.org/10.1029/2020GL091651>
- 441 Summons, R. E., Amend, J. P., Bish, D., Buick, R., Cody, G. D., Des Marais, D. J., et al. (2011).
442 Preservation of Martian Organic and Environmental Records: Final Report of the Mars
443 Biosignature Working Group. *Astrobiology*, 11(2), 157–181.
444 <https://doi.org/10.1089/ast.2010.0506>
- 445 Thomas, N., Cremonese, G., Ziethe, R., Gerber, M., Brändli, M., Bruno, G., et al. 2017. The
446 Colour and Stereo Surface Imaging System (CaSSIS) for the ExoMars Trace Gas Orbiter.
447 *Space Sci. Rev.* 212, 1897–1944. <https://doi.org/10.1007/s11214-017-0421-1>
- 448 Westall, F., Foucher, F., Bost, N., Bertrand, M., Loizeau, D., Vago, J. L., et al. (2015).
449 Biosignatures on Mars: What, Where, and How? Implications for the Search for Martian
450 Life. *Astrobiology*, 15(11), 998–1029. <https://doi.org/10.1089/ast.2015.1374>
- 451 Williams, R. M. E., Irwin, R. P., & Zimbelman, J. R. (2009). Evaluation of paleohydrologic
452 models for terrestrial inverted channels: Implications for application to Martian sinuous
453 ridges. *Geomorphology*, 107(3-4), 300–315.
454 <https://doi.org/10.1016/j.geomorph.2008.12.015>
- 455 Williams, R.M.E., Grotzinger, J.P., Dietrich, W.E., Gupta, S., Sumner, D.Y., Wiens, R.C., et al.,
456 2013, Martian fluvial conglomerates at Gale crater: *Science* 340, 1068–1072,
457 <https://doi.org/10.1126/science.1237317>.
- 458 Vago, J. L., Westall, F., Pasteur Instrument Teams, Coates, A. J., Jaumann, R., Korablev, O., et
459 al. (2017). Habitability on early Mars and the search for biosignatures with the ExoMars
460 rover. *Astrobiology*, 17, 471–510. <https://doi.org/10.1089/ast.2016.1533>
- 461 Zaki, A. S., Pain, C. F., Edgett, K. S., & Castelltort, S. (2021). Global inventory of fluvial ridges
462 on Earth and lessons applicable to Mars. *Earth-Science Reviews*, 216.
463 <https://doi.org/10.1016/j.earscirev.2021.103561>
- 464 Zuber, M. T., Smith, D. E., Solomon, S. C., Muhleman, D. O., Head, J. W., Garvin, J. B., et al.
465 (1992). The Mars Observer laser altimeter investigation. *Journal of Geophysical*
466 *Research*, 97, 7781–7797. <https://doi.org/10.1029/92JE00341>
- 467
468